

Self-Healable and Recyclable Tactile Force Sensors with Post-Tunable Sensitivity

Xiaozhuang Zhou, Xuan Zhang, Huaixia Zhao, Baiju P. Krishnan, and Jiaxi Cui*

It is challenging to post-tune the sensitivity of a tactile force sensor. Herein, a facile method is reported to tailor the sensing properties of conductive polymer composites by utilizing the liquid-like property of dynamic polymer matrix at low strain rates. The idea is demonstrated using dynamic polymer composites (CB/dPDMS) made via evaporation-induced gelation of the suspending toluene solution of carbon black (CB) and acid-catalyzed dynamic polydimethylsiloxane (dPDMS). The dPDMS matrices allow CB to redistribute to change the sensitivity of materials at the liquid-like state, but exhibit typical solid-like behavior and thus can be used as strain sensors at normal strain rates. It is shown that the gauge factor of the polymer composites can be easily post-tuned from 1.4 to 51.5. In addition, the dynamic polymer matrices also endow the composites with interesting self-healing ability and recyclability. Therefore, it is envisioned that this method can be useful in the design of various novel tactile sensing materials for many applications.

and FA-II) measure the dynamic force.^[7–9] Such complex system allows skin to tune its sensitivities to perceive a wide range of mechano-stimuli. To fully construct such capability of human skin for various applications, several strategies have been developed to fabricate flexible tactile force sensors with tunable sensitivity,^[10–14] such as tailoring the material compositions of conductive polymer composites^[10,11,14] or controlling the structure of the materials.^[15–17] However, these strategies suffer from high costs, complicated fabrication processes, poor controllability, and limited tunable range of sensing range, which hinder their practical applications.^[18,19] Therefore, a facile method to precisely tune the force-sensing property of flexible tactile sensors in a large range is still desirable.


1. Introduction

Electronic skin (E-skin) is attracting more and more attention because of their potential applications in soft robotics,^[1] prosthetics,^[2,3] health monitoring,^[4,5] and various wearable devices.^[6] It is designed to mimic the sophisticated human somatosensory system by transducing external stimuli (such as heat, light, mechano-force, and humidity) into electrical signals. Essential to this transduction, flexible materials that could sense tactile force should be built into E-skin to mimic the force-sensing ability of the human skin. Human skin contains four kinds of mechanoreceptors to realize different characteristics of force perception, that is, two slow adapting receptors (SA-I and SA-II) response to static force and two fast adapting receptors (FA-I

In addition to tunable sensitivity, the recoverability of sensing functions or even full recyclability after the tactile force sensor is damaged is another important property for practical applications. Introducing these capabilities into flexible tactile force sensors can significantly elongate their service time and then reduce waste. To this end, both concepts of self-healing^[20] and recycling^[21] are applied to fabricate flexible force sensors by using the composites made from dynamic polymer matrices (dynamic composites), leading to the creation of many self-healable or/and recyclable sensors. Despite this progress, it is still a challenge to combine these capabilities to tactile force-sensing materials that could precisely tailor the sensitivity.

Here, we report a strategy for post-tuning the sensitivity of flexible strain-sensing materials used for tactile force sensors. This strategy is based on the utilization of the unique mechanical properties of dynamic polymer networks (**Figure 1a**), that is, showing liquid-like behavior (storage modulus (G') < loss modulus (G'')) at an extremely low strain rate due to the reconfiguration of polymer networks but solid-like behavior ($G' > G''$) at a normal strain rate (5–400 Hz).^[22,23] In practical applications, the solid-like polymer matrices could fix conductive particles dispersed inside to show strain-sensitivity, that is, reversibly breaking the conductive pathways under a strain (**Figure 1b,c**). In the liquid-like state, the polymer matrices would allow conductive particles entrapped in the matrices to redistribute when the sample is deformed.^[24–30] And we assume that such redistribution of conductive particles should lead to significant change in the strain sensitivity. A polymer composite consisting of carbon black (CB) and dynamic covalent polydimethylsiloxane (dPDMS) elastomer (**Figure 1d**) is designed to demonstrate this

X. Zhou, Dr. X. Zhang, Dr. H. Zhao, Dr. B. P. Krishnan, Prof. J. Cui
INM – Leibniz Institute for New Materials
Campus D2 2, Saarbrücken 66123, Germany
Prof. J. Cui
Institute of Fundamental and Frontier Sciences
University of Electronic Science and Technology of China
Chengdu, Sichuan 610054, China
E-mail: jiaxi.cui@uestc.edu.cn

 The ORCID identification number(s) for the author(s) of this article can be found under <https://doi.org/10.1002/adfm.202003533>.

© 2020 The Authors. Published by WILEY-VCH Verlag GmbH & Co. KGaA, Weinheim. This is an open access article under the terms of the Creative Commons Attribution License, which permits use, distribution and reproduction in any medium, provided the original work is properly cited.

DOI: 10.1002/adfm.202003533

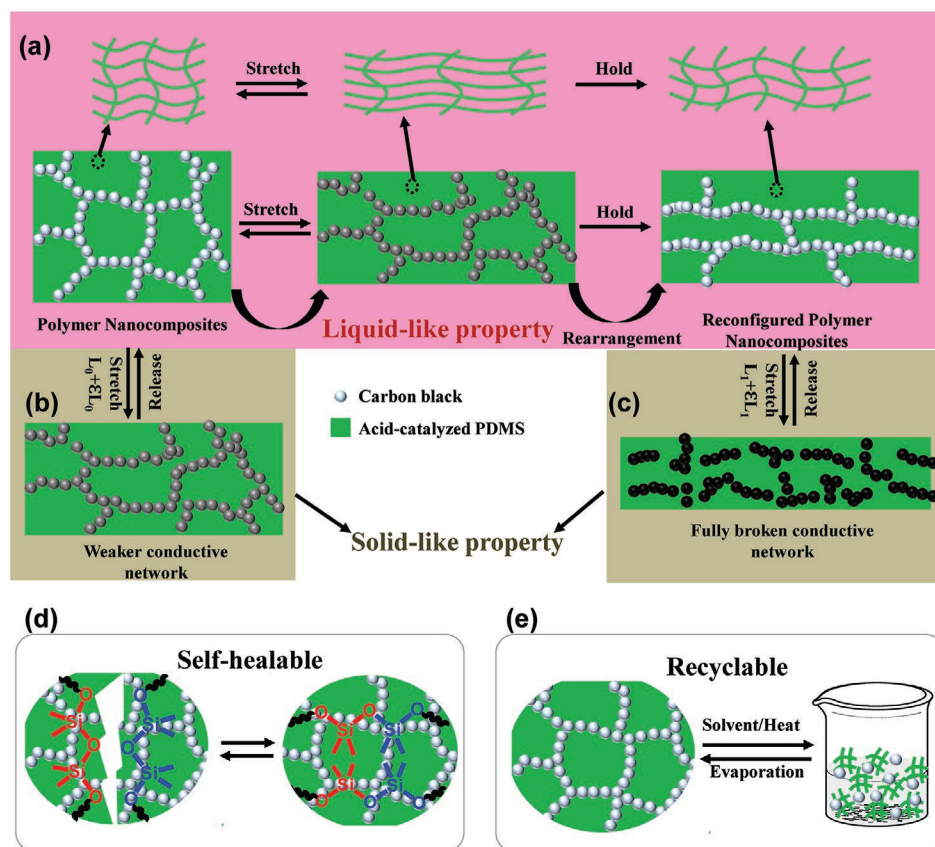


Figure 1. Schematic design of tailoring the sensitivity and sensing range by mechanical stretching a) Liquid-like property at a fixed strain where the reshuffle of the polymer chain and rearrangement of particle networks can occur. The electrical response of sensors made b) from the composites and c) from the reconfigured polymer composites at normal strain rates. d) The self-healing mechanism of the CB/dPDMS composites. e) Recycling mechanism of the CB/dPDMS composites.

assumption. In the presence of acid catalyst, the silicone is in an equilibrium state. On-going chain exchanges occur at room temperature, which enable not only reorganization of CB in a relaxation process but also self-healing behavior after damage. The equilibrium of siloxane matrices can also be utilized to induce depolymerization for recycling the materials (Figure 1e).

2. Results and Discussions

2.1. Preparation and Properties of CB/dPDMS Composites

The CB/dPDMS composite was prepared through evaporation-induced gelation process of the suspending solution of CB in the mixture of octamethylcyclotetrasiloxane (D_4 , monomer), 1,1,1-tri(2-heptamethylcyclotetrasiloxane-yl-ethyl)-methylsilane ($triD_4$, crosslinker), triflic acid (catalyst), and toluene (solvent). A toluene solution was designed because CB could disperse well in it. In the solution, D_4 and $triD_4$ could undergo acid-catalyzed ring opening copolymerization to form siloxane network clusters. In the presence of triflic acid, the siloxane was in equilibrium state.^[31] Therefore, with evaporation of toluene, these siloxane clusters integrated together to form an elastic composite. Such evaporation-induced gelation process allowed us to prepare the composite to various shapes in different scales via

facile casting or molding methods. The obtained composite is denoted as $CB(x)/dPDMS(y)$ where x is the weight percentage (%) of CB in the composite and y is the weight concentration of crosslinker in dPDMS. **Figure 2a** displays a specimen of $CB(1)/dPDMS(1)$ with a diameter of 5 cm prepared in a petri dish.

Scanning electron microscopy (SEM) was used to study the morphology of the obtained composite. **Figure 2b** shows the cross-section of $CB(1)/dPDMS(1)$ composites. A fractal structure was observed, in which the aggregates of CB particles were connected together to form networks in the dPDMS matrix. Similar fractal structures formed in all test samples with different CB contents (0.5–10 wt%, **Figure S1a**, Supporting Information). We attributed the formation of such conductive networks to the synergic consequence of acid-induced aggregation of CB and solvent evaporation-induced gelation. CB particles could disperse well in the toluene solution without acid. Addition of acid into the solution not only trigger polymerization but also induce aggregation of CB particles, since CB particles would absorb acid molecules on their surface to increase surface hydrophilicity.^[32] The aggregation was accompanied with toluene evaporation and accumulative structures were then fixed in the gelation process. Here we expected the alternation of surface hydrophobicity, rather than the increase of polymer fraction, led to the aggregation. Control experiments were conducted to confirm this idea (**Figure S1b**, Supporting Information).

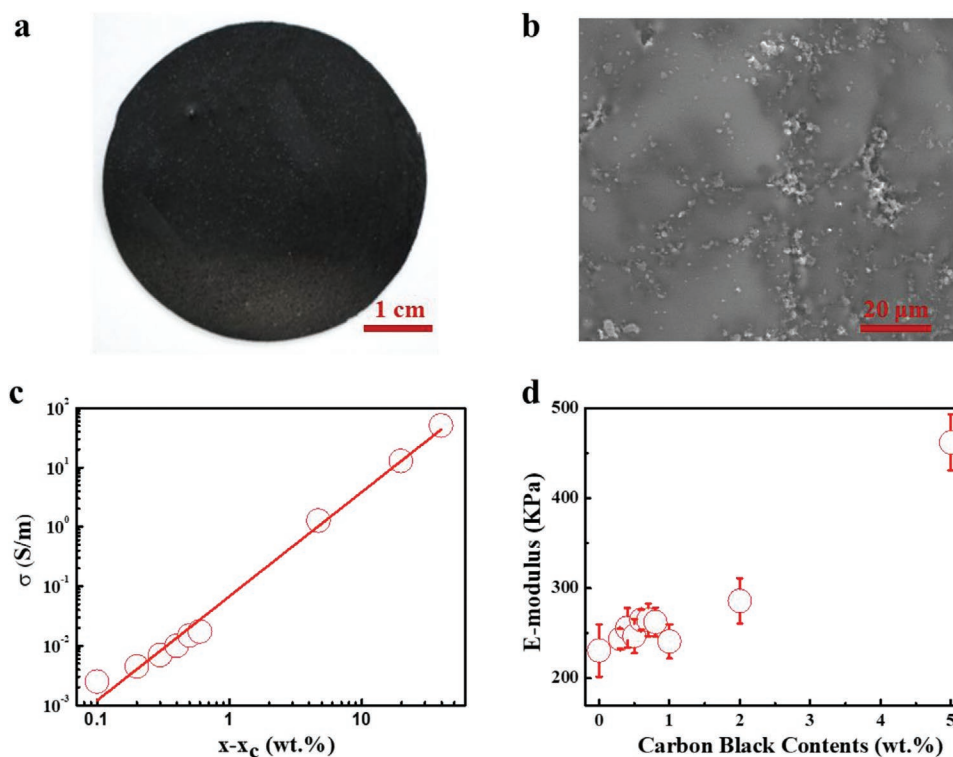


Figure 2. Structure and properties of CB/dPDMS composites. a) Photograph of an as-prepared CB(1)/dPDMS(1) film. b) SEM cross-section image of the CB(1)/dPDMS(1) composites showing a network of carbon black particles. c) Electrical conductivity of CB/dPDMS(1) composites as a function of the parameter $x - x_c$, where x is the weight fraction and x_c is the electrical percolation threshold. d) E-modulus of CB/dPDMS(1) composites with different CB contents.

To a suspending solution of CB in the mixture of toluene and D_4 , crosslinkable PDMS or acid was added. It was found that the addition of acid induced fast sedimentation of CB but addition of PDMS did not. To further confirm the absorption of acid molecules on the surface of particles, we have measured the zeta potential of the CB particles after acid-treatment. In our additional experiment, the CB particles after acid-treatment in toluene were collected and re-dispersed in water for avoiding the influence of suspending acid droplets in toluene. It was found that the zeta potential jumped from -274 ± 0.69 to 3.77 ± 0.70 mV after acid-treatment. The results were supporting our proposed mechanism in which acid molecules were absorbed on CB particles by bonding protons on the surfaces.

The conductivity (σ_e) of CB/dPDMS composites with different filler concentrations was measured (Figure 2c). An exponential relationship between the conductivity and the filler concentration was observed, which can be described by the equation:^[33]

$$\sigma_e \propto (x - x_c)^{n_e} \quad (1)$$

where x is the weight fraction of the filler, x_c is the critical weight fraction at the percolation threshold and n_e is the scaling exponent relating to the weight fraction. Analysis of the data in Figure 2c using Equation (1) yields a percolation threshold of 0.3 wt% and an exponent $n_e = 1.74$. The exponent is very close to the theoretical value of 3D conductive networks ($n_e = 2$).^[34] It was attributed to the formation of CB conductive networks within the

polymer composites. Note that the critical fraction (x_c) is remarkably lower than previously reported values (3–20 wt% for CB/PDMS composites).^[35] It could also be explained by the aggregated CB conductive network structure which made the polymer composites conductive even at a relatively low concentration.

Figure 2d shows the tensile E-modulus (Young's modulus) of the samples. The pristine dynamic PDMS exhibits an E-modulus of 230 ± 29 KPa. The addition of low loading CB (0.3–1 wt%) into the matrices scarcely increases their E-modulus. Clear mechanical reinforcement was observed when the filler content was up to 2 and 5 wt% (285 ± 25 and 462 ± 31 KPa, respectively). In addition, the modulus of CB/dPDMS could be remarkably tuned by varying the crosslinking degree of the dPDMS matrix (e.g., from 0.1 to 5 wt%; Figure S2, Supporting Information).

2.2. Sensing Properties of CB/dPDMS Composites

The electrical resistance response of the CB/dPDMS composites to the force at the solid-state was investigated. It is known that the sensing property of the dynamic polymer composites is related to the viscoelastic property.^[24] We thus assumed that CB content should be a good parameter to tune the sensing property since the viscoelastic property of the CB/dPDMS composites varied with it. Samples of CB(x)/dPDMS(1) where x ranges in 0–2 wt%, were prepared for this study. The storage modulus (G') is higher than loss modulus (G'') for all the samples in the tested frequency range of 0.0628–157 rad s^{-1} (Figure S3,

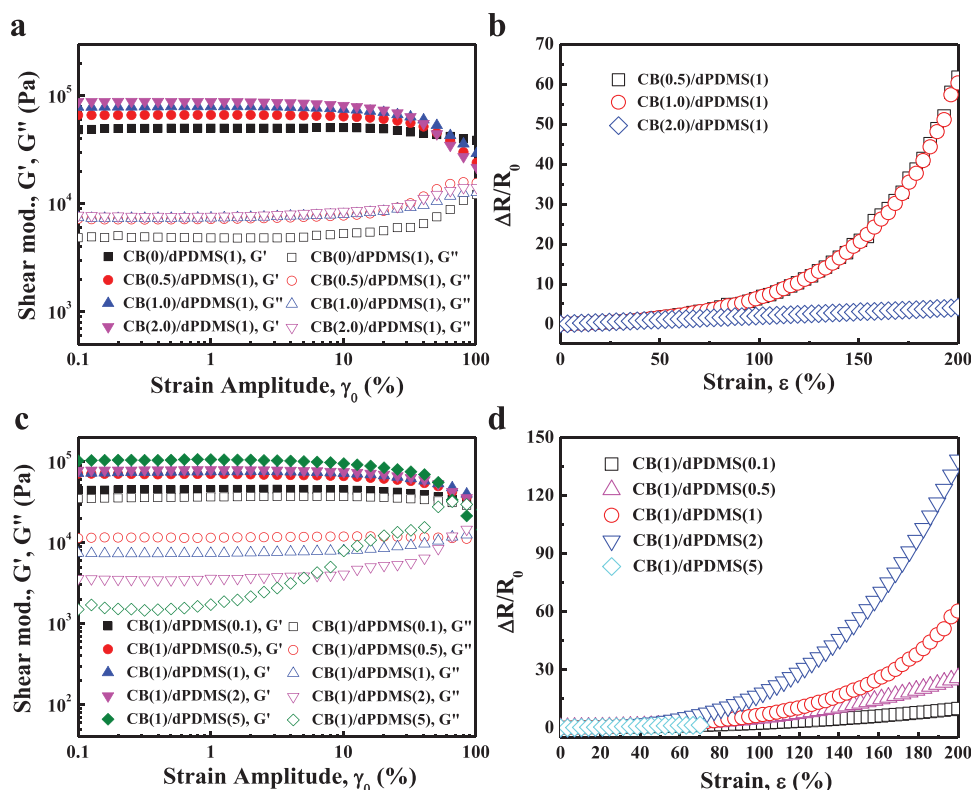


Figure 3. Mechanical and sensing properties of the CB/dPDMS composites. a) G' and G'' versus the oscillation strain amplitude for the CB(x)/dPDMS(1) composites with different CB ($\omega = 6.28 \text{ rad s}^{-1}$). b) Electrical response of the sensors, made from CB(x)/dPDMS(y) composites with different CB contents (Loading rate: 20 mm min^{-1}). c) Shear storage (G') and loss (G'') moduli of CB(1)/dPDMS(y) composites as a function of oscillation strain amplitude with different crosslinker contents ($\omega = 6.28 \text{ rad s}^{-1}$). d) Electrical response of the sensors, made from CB(1)/dPDMS(y) composites, versus the strain (Loading rate: 20 mm min^{-1}).

Supporting Information), implying typical solid-like feature at the normal strain rates. In our test condition (strain amplitude: 0.1–100%; frequency: 6.28 rad s^{-1}), the G' and G'' of CB($x \leq 2$)/dPDMS(1) with different x display similar curves, that is, stable in low amplitude and showing a shear softening in high amplitude (decrease in G' but increase in G'' , Figure 3a). The softening of the polymer composites could be attributed to either the breakage of filler networks (Payne's effect) or polymer chains. We assigned the softening in our case to the breaking of polymer chains, rather than Payne's effect, because of the following three reasons: 1) the polymer matrix (dPDMS) also displays the similar strain softening behavior; 2) the CB contents in our composites is low ($<2 \text{ wt}\%$) and its contribution to the mechanical property is quite small, as indicated by Figure 2d; 3) the Payne's effect is normally observed in small strain range ($<20\%$), but in our case, the softening occurs in the strain larger than 20%. In addition, the similar curves of G' and G'' suggested that the addition of CB in the range of $<2\%$ has negligible effect on the viscoelasticity of the polymer composites, though slightly increase of both G' and G'' was observed.

The sensing property of CB(x)/dPDMS(1) was investigated. Electrical resistance (R) of as-prepared CB/dPDMS composites at a loading rate 20 mm min^{-1} was collected to evaluate their response to strain (Figures S4 and S5, Supporting Information). Figure 3b shows the relative resistance change, $\Delta R/R$, of the CB/dPDMS composites with strain. The CB(0.5)/dPDMS(1)

and the CB(1)/dPDMS(1) display nearly the same $\Delta R/R$ - ϵ curves, indicating that the CB contents less than 1% has negligible effect on the sensing property of the CB/dPDMS composites. This could be attributed to the similar viscoelasticity of the samples with $<1\%$ CB. In addition, the exponential variation of $\Delta R/R$ implies that the conductive network was broken during the stretching, as indicated in the graphene putty.^[24] When the CB content was further increased to 2 wt%, $\Delta R/R$ increased linearly with strain, showing significantly different change from the CB (0.5 or 1)/dPDMS(1). The sensitivity can be quantitatively described by the gauge factor (GF, defined as $\text{GF} = (\Delta R/R)/\epsilon$, where $\Delta R/R$ and ϵ are relative resistance change and applied strain, respectively). The GF of CB(2)/dPDMS(1) is about 2.13. This small GF indicated that the resistance change was attributed to geometry change of the sample, rather than the breaking of conductive CB network under the strain. In other words, stretching could not break the connected CB network for the CB(2)/dPDMS composites. It might due to the strong CB network interaction made from high CB loading such that the CB network could resist the stretching.

The viscoelasticity and sensitivity of CB(x)/dPDMS(y) also varied with y (crosslinker content). Samples of CB(1)/dPDMS(y) where y is tuned from 0.1% to 5%, were prepared for this study. They all display the solid-like feature ($G' > G''$) in the tested frequency range of 0.0628 – 157 rad s^{-1} (Figure S6, Supporting Information). As shown in Figure 3c, the samples with various

crosslinker display significantly different curves, especially those of G'' , indicating that crosslinking degree was an efficient parameter to tune the viscoelastic property of the CB/dPDMS composites. The sensing property of the CB(1)/dPDMS(γ) was also measured at the loading rate of 20 mm min⁻¹ (Figure 3d). It was found that $\Delta R/R$ of CB(1)/dPDMS(γ) with 0.1% $\leq \gamma \leq 2\%$ increased exponentially with strain and the sensitivity increases with γ . This phenomenon could be explained by the R-strain model, assuming that $\Delta R/R$ is the conflicting effect of forced-induced breaking of the conductive network and viscous polymer matrix-induced reforming of the CB network.^[24] The force-induced breaking of the conductive particles is assumed to increase the resistance while rearrangement of the CB particle would decrease the resistance. Since increasing crosslinking degree enhanced the solid feature of the samples (Figure 3c), the resistance change is more pronounced in CB(1)/dPDMS(γ) with higher γ . CB(1)/dPDMS(5) displays a linear increase of $\Delta R/R$ with a GF of 1.98 (Figure 3d), indicating that the connected CB network was not broken during stretching. Since CB(1)/dPDMS(5) behaved more like a good elastomer (low G'' , Figure 3c), the unbroken CB network under stretching could be explained by one potential reason that the elastic polymer composites could not have the Payne's effect as the viscoelastic polymer composites, breaking of the particle interaction under stretching.^[36]

2.3. Tuning the Sensitivity of the CB/dPDMS Composites

CB(1)/dPDMS(1) was selected to demonstrate the modulation of sensitivity via mechanical treatment. We first checked the liquid-like feature of the sample at the low strain rates by rheological measurements starting from a frequency of 5×10^{-4} rad s⁻¹ (Figure 4a). At the frequency lower than 8×10^{-4} rad s⁻¹, the loss modulus is higher than the storage modulus, implying a liquid-like state, while at the frequency of $>8 \times 10^{-4}$ rad s⁻¹, the sample shows a higher storage modulus, indicating a solid-like state. Such unique mechanical property of CB(1)/dPDMS(1) allows it to behave as a normal solid in the absence of stimuli so that they can maintain the original shapes but like a liquid under constant pressure to allow the redistribution of the CB particles (Figure 4b). Under the constant pressure, stress relaxation occurred in CB/dPDMS via chain exchange to induce permanent deformation. The strain rate was automatically tuned to the level allowing liquid-like behavior. Stress relaxation measurement was conducted to study the reconfiguration rate of CB/dPDMS composite (Figure S7, Supporting Information). As shown in Figure 4c, the stress was completely relaxed in 4.5 h, leading to a permanent deformation. During this relaxation, redistribution of CB particles was expected. To confirm this, the resistance was tracked during the stress measurement (Figure 4c). The resistance jumped to a high value when the sample was stretched. In the process of stress relaxation with constant strain, the resistance gradually decreased. The jump was attributed to the disconnection of the CB network in straining while the decrease was assigned to the rearranging of CB particles to reform a new connecting structure. Upon a strain, the polymer matrices significantly deform, which immediately led to the breaking of CB networks.^[24]

In this case, the polymer chains were stretched into an entropy-unfavorable extending state, which drove the polymer chains to exchange to go back to relaxed conformation. The reformation of the CB networks depended on the reconfiguration of the dynamic matrices which was slow. The rearrangement of the CB particles was also supported by SEM results in which the morphology of CB network structure changed after the relaxation (Figure S8, Supporting Information). Such force-induced particle rearrangement has been found in graphene putty and Ag flakes/PDMS-4,4'-methylenebis(phenyl urea) (MPU)_{0.4}-isophorone bisurea units (IU)_{0.6} polymer composite,^[24,25] but high hysteresis effect was observed in the materials, making them not suitable to be used for the reconfigurable sensors.

The rearrangement of CB network under a fixed strain was utilized to tune the sensor property. To demonstrate this concept, CB(1)/dPDMS(1) was stretched to different strains to create different arrangement of CB particles. Cyclic tensile stress-strain measurement was used to study the mechanical properties of the as-prepared and reconfigured composites at a high strain rate. Under a loading rate of 20 mm min⁻¹, small hysteresis loops were observed in the cyclic tensile test with a strain of 50% (black solid line in Figure 4d), implying a typical elastic behavior. Such an elastic feature at normal strain rates indicated that the CB/dPDMS composites could be a good candidate for tactile sensors since mechanical hysteresis is undesired in sensing strain.^[37,38] The same mechanical properties of the 150% strain-deformed samples (red short dot line in Figure 4d) suggested that the reconfigured CB(1)/dPDMS(1) composites could still be used as tactile force sensors. Here the reconfigured composites were denoted as n-rCB(x)/dPDMS (y) where n is the strain used in stress relaxation. The resistivity of the reconfigured composites increases with applied strain (Figure S9, Supporting Information). The sensing property of the obtained materials were then collected at a loading rate of 20 mm min⁻¹, with an as-prepared CB/dPDMS sample as the control (Figure 4e). As expected, all the rCB/dPDMS display faster responsiveness to mechanical stimuli than the intact sample. Moreover, increasing the strain used for stress relaxation enhanced the sensitivity of the reconfigured CB/dPDMS composites. On the other hand, the sensing range also varied with the strain (n in n-rCB/dPDMS).

Generally speaking, the sensitivity of the sensors increased when the fixed strains went up. Since the reconfiguration process has no effect on the mechanical property of the polymer composites (Figure 4d), there must be other reason rather than the change of viscoelasticity that underlies the phenomenon. It is already reported in literature that the distribution of interparticle connections can lead to different percolation exponents that would be intimately related to the sensitivity of the conductive composites upon strain.^[34] The sufficient widely distributed interparticle connections could even show non-universal property, giving a percolation exponent greater than 2 in the 3D network and the resulting resistance-strain curves could be logarithmically divergent, which has been demonstrated both theoretically and experimentally.^[39] We attributed such tailorable sensor property to the on-demand redistribution of interparticle connections.^[40] To demonstrate this, the R-strain model describing the resistance change versus strain for dynamic covalent polymer composites was applied in our

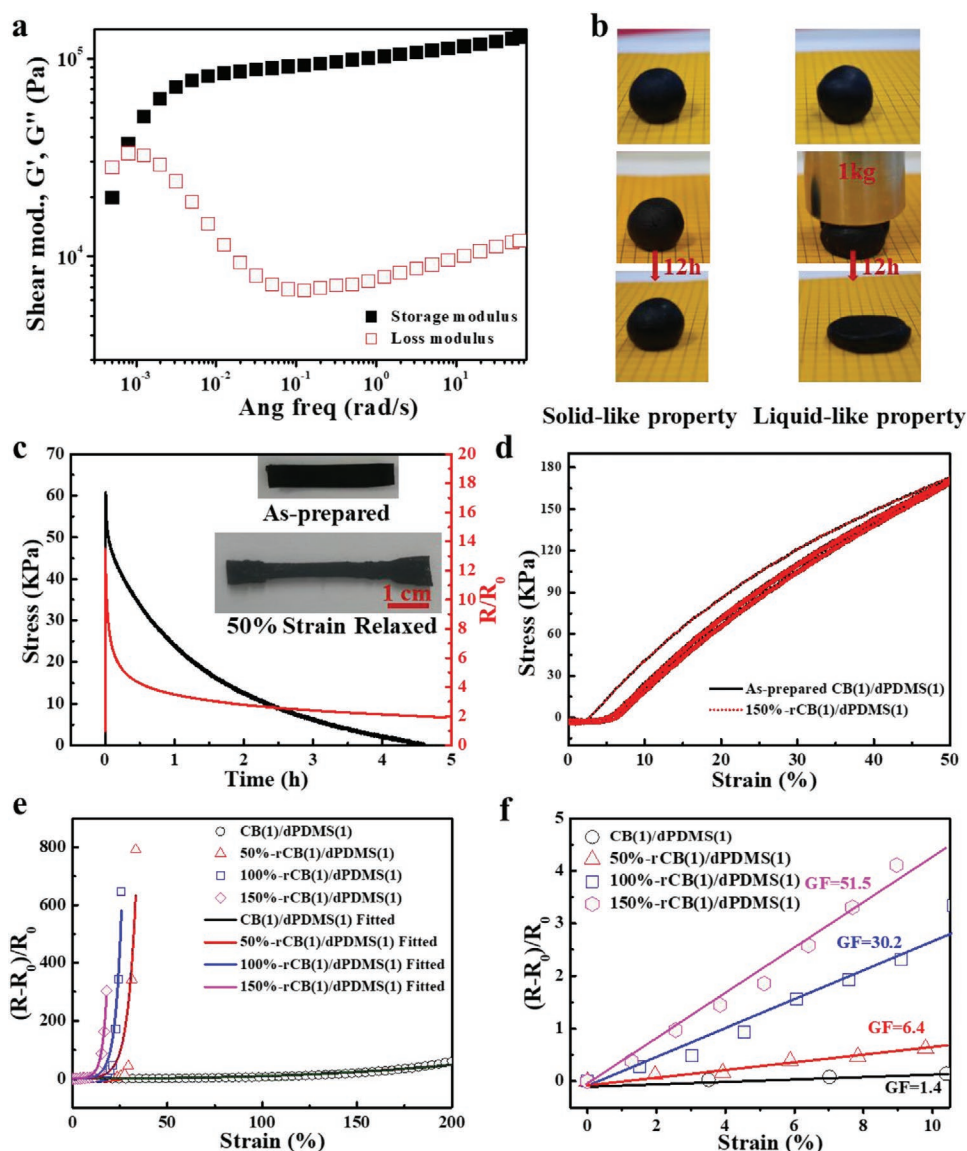


Figure 4. Mechano-tailorable sensitivities of the CB/dPDMS composites. a) Angular frequency dependence of storage modulus and loss modulus for the CB(1)/dPDMS(1). b) Pictures demonstrating the solid-like property in the absence of external stimuli and liquid-like property when there is a constant pressure. A CB(1)/dPDMS(1) was used. c) Stress relaxation and electrical resistance tracking of the CB(1)/dPDMS(1) at the fixed strain of 50%. Inset displays a CB(1)/dPDMS(1) sample before and after the stress-relaxation. d) Cyclic stress-strain curves for the CB/dPDMS and 150%-strain reconfigured CB(1)/dPDMS(1) at the loading rate of 20 mm min^{-1} . e) Electrical resistance change versus strain of the sensors made from CB(1)/dPDMS(1) composites and the strain-reconfigured CB(1)/dPDMS(1) at a loading rate of 20 mm min^{-1} . The symbols are the experimental results and the solid lines are the simulated results. f) Gauge factors of the sensors made from CB(1)/dPDMS(1) composites and the strain-reconfigured CB(1)/dPDMS(1) composites within the small strain deformation (10%).

case.^[24] The resistance change versus the applied strain is as follows:

$$\frac{R}{R_0} = \left[\left(1 + \left(\frac{\varepsilon}{\varepsilon_c} \right)^{2m} \right)^{-1} + k_2 t / N_0 \right]^{-n_\varepsilon} (\varepsilon + 1)^2 \quad (2)$$

where ε_c is the yield strain of the polymer composite, k_2 is the reforming constant due to particle arrangement within the viscous polymer matrix, m is the filler network structure factor, t is the time, n_ε is the conductivity scaling exponent, and N_0 is the initial

number of interparticle connections per volume. In our case, it was assumed that the polymer composites were elastomers that the CB particles were not able to mobile at normal strain rate. An approximate situation was made by setting $k_2 = 0$ in Equation (2) to attain

$$\frac{R}{R_0} = \left[\left(1 + \left(\frac{\varepsilon}{\varepsilon_c} \right)^{2m} \right)^{-1} \right]^{-n_\varepsilon} (\varepsilon + 1)^2 \quad (3)$$

By fitting the experimental data in Figure 4e with Equation (3) ($m = 0.7$ and $\varepsilon_c = 0.8$), the fitting curves agreed

well with the experiment data and we attained $n_c = 1.2$ for the as-prepared sensor and $n_c = 22.8, 31.8,$ and 45.9 for the 50%-rCB(1)/dPDMS(1), 100%-rCB(1)/dPDMS(1) and 150%-rCB(1)/dPDMS(1), respectively. Note that n_c was the scaling exponent of connectivity while n_w was the scaling exponent of weight fraction, but they both represent the distribution of interparticle distances. Therefore, the higher sensitivity of the sensors could be attributed to the broader distributions of the CB interparticle distances in reconfigured CB/dPDMS composites.

Although the electrical resistance changes exponentially with the strain, the resistance change could be approximated as the linear change versus the strain when the deformation is sufficient small. For our as-prepared CB(1)/dPDMS(1) composites and reconfigured materials, the resistance changes linearly within strain in tested range (10%), as shown in Figure 4f. The gauge factor for the as-prepared CB(1)/dPDMS(1) composites is 1.4, and it jumps to 6.4, 30.2, or 51.5 after relaxation at a stretching state of 150%, 200%, or 250%, respectively.

We also evaluated the stability of the samples. Triflic acid is volatile but in our system CB particles could stabilize the acid molecules via bonding them on surface. Therefore, good stability was expected. To confirm this, we stored CB(1)/dPDMS(1) composites for one month and then tested their capability to change sensitivity. Similar plastic deformation and sensitivity change were observed (Figure S10, Supporting Information), supporting our hypothesis.

2.4. Self-Healing of the CB/dPDMS Composite

Strong acid was used to initiate the ring-opening polymerization of the monomer and the ionic propagating species in resulted products retain activity after polymerization, inducing a dynamic equilibration of the siloxane matrix. It was assumed that such dynamic equilibration would bring about interesting self-healing at room temperature. To confirm this idea, the intact CB(1)/dPDMS(1) composites were tentatively cut by a knife and then stored in a sealed vial for observation. As shown in Figure 5a, the cut interfaces disappear after 24 h, implying a recovery in the material's integration. Tensile measurements were used to quantitatively evaluate mechanical self-healing efficiency. The uniaxial tensile stress–strain curves of the healed samples agree well with the intact ones and a healing efficiency of 97% was obtained, estimating by the rupturing energy (Figure 5b). More than the recovery in mechanical properties, the electrical properties such as conductivity and sensing properties are also fully restored (Figure 5c,d). The cut turns off the current of the sample under voltage (3 V) which jumps back after healing. This restoration in current is reversible (Figure 5c). A direct current-powered circuit connecting a light-emitting diode (LED) was further constructed to demonstrate the self-healing of electronic property (Figure S11, Supporting Information). The circuit was died out when being cut and was lit up again after being self-healed. Assembling the intact and self-healed composites to sensors and measure the R-strain curves at the speed of 20 mm min^{-1} , the sensing property of the

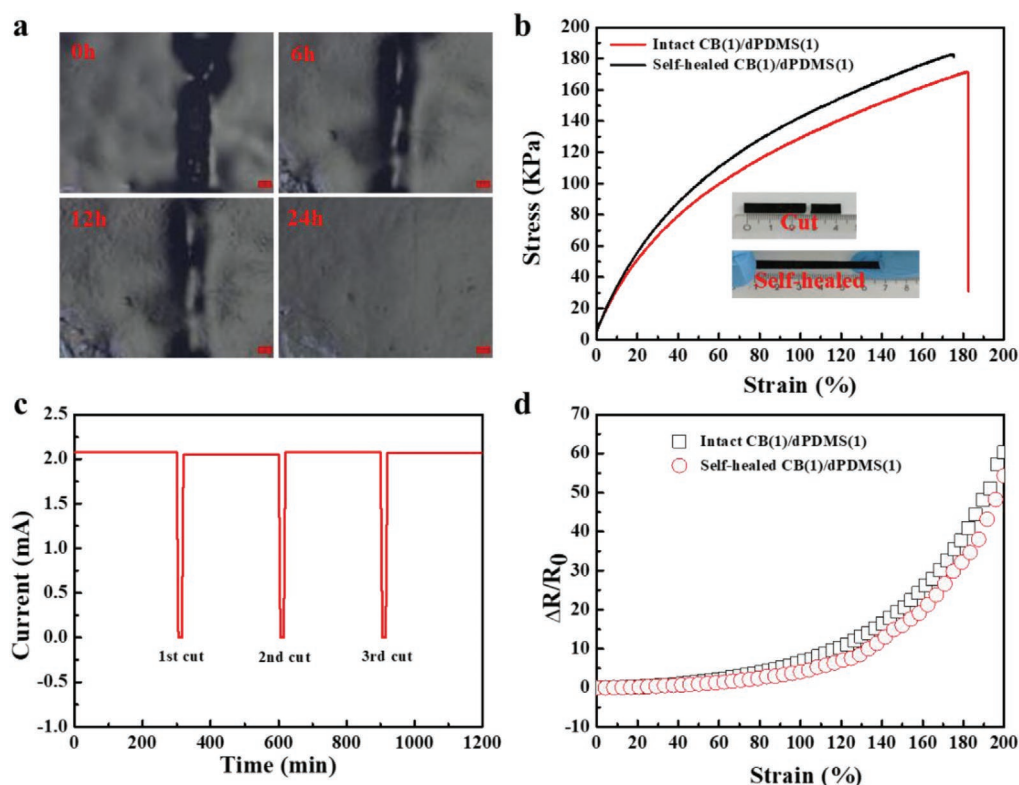


Figure 5. Self-healing of the CB/dPDMS composites. a) Optical images of the cut interface of the composites at different times. Scale bar: 100 μm . b) Stress–strain curves of the self-healed and intact specimens. c) The currents for the intact composites and the self-healed ones. d) The sensor property for the intact sensors and the self-healed ones (loading rate: 20 mm min^{-1}). A CB(1)/dPDMS(1) was used for demonstration.

self-healed sensor agrees well with the intact sensor, indicating a good recovery of the sensor properties (Figure 5d).

2.5. Recycle of the CB/dPDMS Composites

It is known that the polymer would depolymerize to oligomers if the polymer-oligomers equilibrium is moved to the oligomer directions (Figure 6a). In fact, the crosslinked materials could be dissolved for reprocessing in the presence of a good solvent for siloxane. In the presence of acid, the PDMS matrix is in an equilibrium state. Immersing the samples in the good solvents of PDMS would drive the equilibrium toward depolymerization, since the depolymerization products are constantly diluted by solvents. Based on this mechanism, the solubility of solvents used for recycle was important. To confirm this, different solvents (*n*-hexane, chloroform, *N*-hexadecane, toluene) have been used to recycle the CB(1)/dPDMS(1) composites. 2 g CB(1)/dPDMS(1) were put in the 15 g solvents. After 24 h, the

composites were dissolved in the *n*-hexane, chloroform, and toluene but not in the *N*-hexadecane, indicating this process is solvent-dependent (Figure S12, Supporting Information).

We demonstrated the recycling mechanism of our materials by subjecting the as-prepared CB(1)/dPDMS(1) composites into toluene (Figure 6b). The composites were completely dissolved after stirring for 12 h (Figure 6b). Analyzing the dissolved solutions by gas chromatography mass spectrometry (GC-MS; Figure S13, Supporting Information) and gel permeation chromatography (GPC, Figure 6c) revealed that the matrix had been completely converted into cyclic oligomers via depolymerization in the toluene solutions. To further confirm the acid-catalyzed depolymerization mechanism, a control experiment was conducted with well-defined PDMS (500 cSt) as a starting material. It was found that in the presence of triflic acid, the linear PDMS could also be converted into oligomers in 12 h (checked by GC-MS and GPC). We also investigated the contribution of CB particles to the depolymerization by a control experiment in which the PDMS oil (500 cSt) and dynamic PDMS elastomer

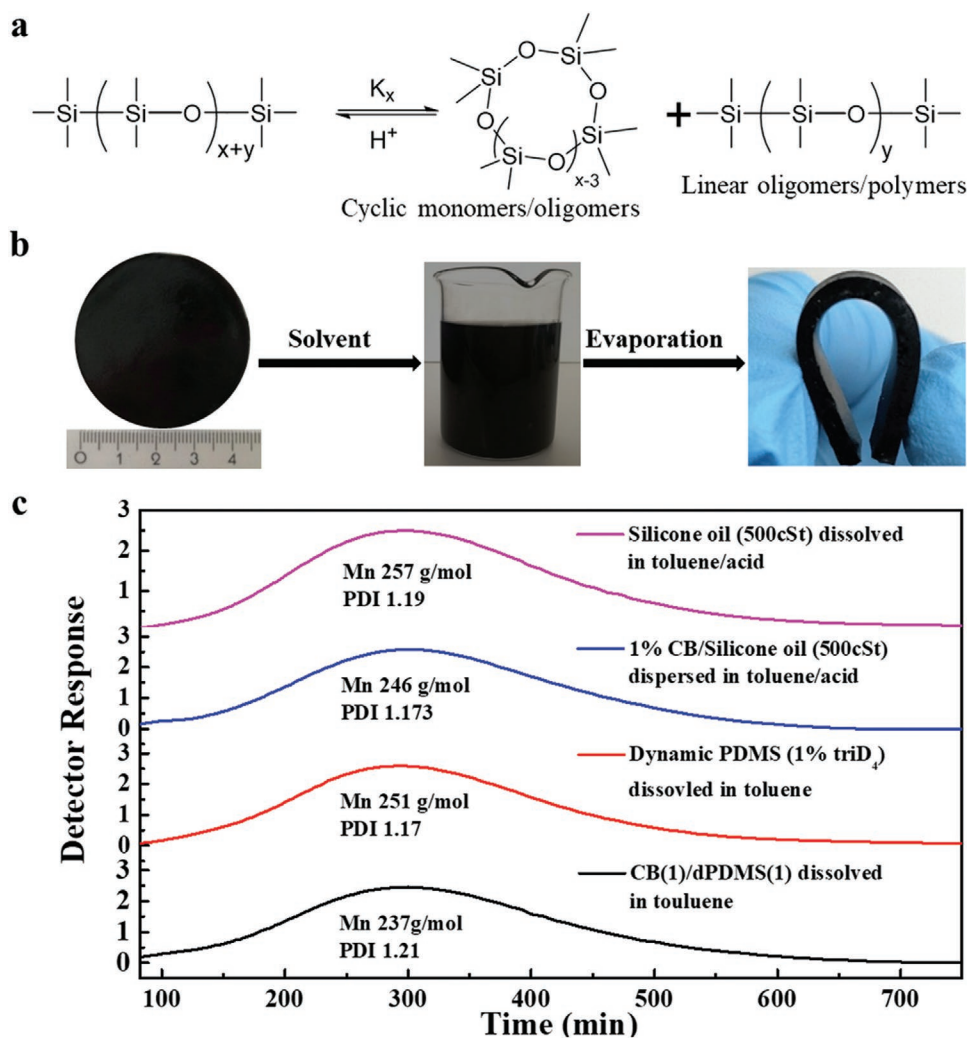


Figure 6. Recycle of the CB/dPDMS composites. a) Polymer-oligomer equilibrium in the acid-catalyzed dynamic PDMS. b) Reprocessing CB/dPDMS composites by dissolving them in toluene and the evaporation of toluene will rebuild the materials. c) GPC analysis of oligomers by dissolving CB/dPDMS, dPDMS (1% triD₄), CB/Silicone oil (500cSt) and silicone oil (500cSt) in toluene. A CB(1)/dPDMS(1) was used in (b) and (c).

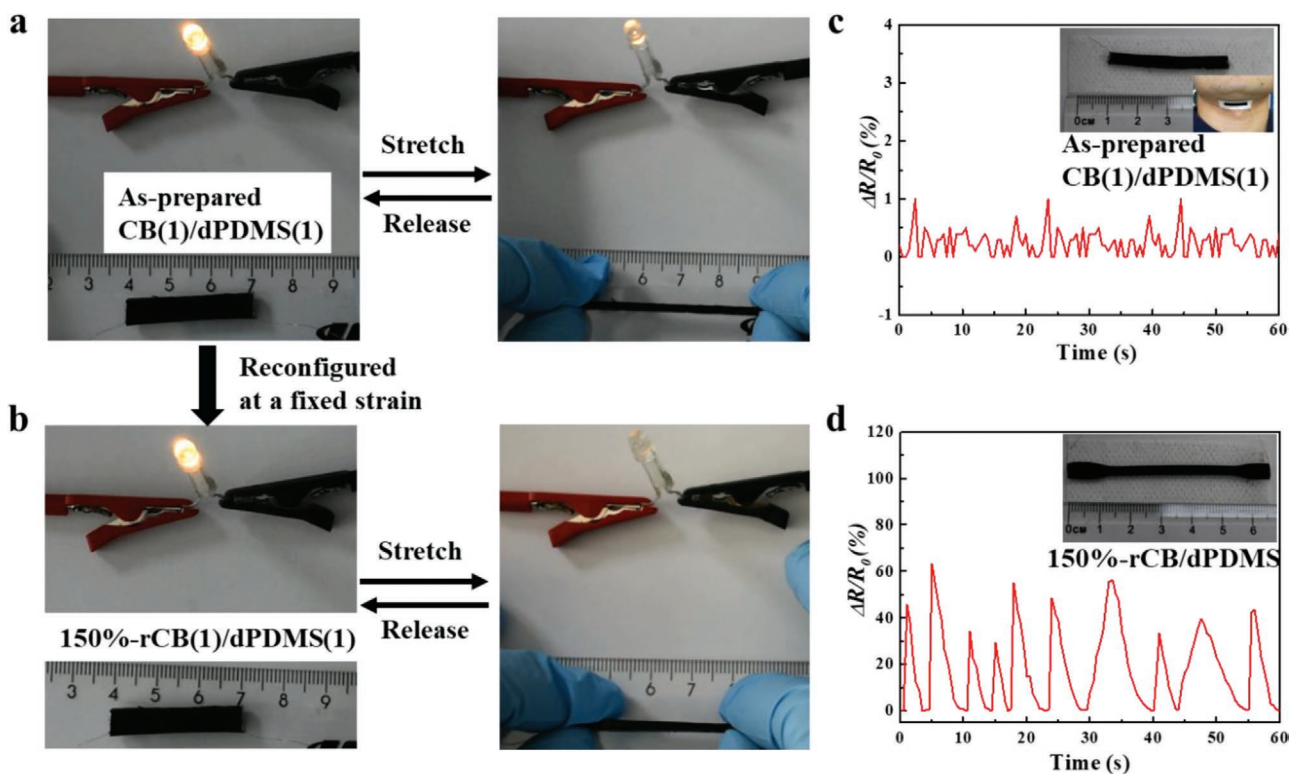


Figure 7. Application of tailorable CB/dPDMS composites. a,b) Demonstrating of different sensing properties for the as-prepared CB(1)/dPDMS(1) and 150%-rCB(1)/dPDMS(1) composites. c,d) On-demand sensing property. The sensors that are not able to detect tiny motions could be reprocessed to be able to work by simple mechanical stretching and holding.

(1 wt% triD₄) did not contain any CB particle were dissolved in the toluene in the presence of triflic acid. Similar results were obtained, indicating that the presence of CB particles was not necessary for the depolymerization of polymers.

2.6. Applications of the Tailorable Sensors

We demonstrated the tailorable sensing property of the CB/dPDMS composites via simple mechanical stretching. To this end, a CB(1)/dPDMS(1) stripe (4 mm × 30 mm) was cut from the large size composites and assembled into circuits with a LED. For the as-prepared sensors, the illumination intensity of the LED reversibly decreased slightly when the stripe was stretched to 180% of its original length (Figure 7a). Stretching the sensors to 150% for 24 h stress relaxation in-situ increased the strain-sensitivity (Figure 7b). The illumination intensity decreased dramatically (totally die out), even the material was slightly stretched (30% strain, Figure 7b). The strain-induced switching was also reversible. Such in-situ modulation of sensitivity implied that our materials could be applied to sense a wide range of mechano-stimuli.

The sensing property of the materials was further tailored to accommodate customized wearable device applications. A flexible human motion detector was fabricated by connecting the assembled sensors to a daily bandage which was used to prevent the direct contact with the skin (Inset in Figure 7c). A PDMS rubber glue (SH-78) was used to bind the assembled

sensors and the bandage to avoid the potential failure. After sticking the bandage onto the skin, the force sensors, the skin, and the bandage would behave as a single cohesive stretchable object, and therefore, the deformation of human-motion could be precisely monitored by the force sensors. Monitoring human tiny motion such as speaking requires a high sensitivity. When the as-prepared CB(1)/dPDMS(1) tactile sensors were attached to the throat to monitor the speaking, no reliable signals was obtained since the low sensitivity of the sensor, as shown in Figure 7c. Instead of replacing the as-prepared sensors in the normal case, simply stretching the as-prepared sensors at a strain of 150% to allow a stress relaxation for 12 h, the sample could re-use to detect the tiny motion to delivery reliable electrical signal (Figure 7d). With this proof-of-concept demonstration, we envisioned that our post-tailorable strain-sensing materials could be used for preparing versatile sensors to alleviate the space usage. Such on-demand modulation could decrease the fabrication difficulties and cost, showing potential in preparing various flexible integrated circuits such as electronic skin, soft robotics, and flexible prosthesis.

3. Conclusion

In summary, we have reported a facile method for post-tuning the sensitivity of flexible conductive polymer composites. In this method, the unique mechanical property of dynamic polymer network, that is, showing a liquid-like behavior to allow

conductive filler to redistribute, has been utilized to modulate the sensitivity. We have demonstrated this concept here by the CB/dPDMS systems and showed that the GF of the composites can be tuned from 1.4 to 51.5 by stretching the grown composites to induce rearrangement of CB particles. In addition to the post-tunable sensitivity, the dynamic of dPDMS also endows the sensor with excellent self-healing ability and recyclability. The methodology developed here is facile and can lead to good sensing performance and excellent mechanical properties. We believe that it can be applicable for different dynamic polymer composites and therefore, envision its application in preparing various tactile sensors.

4. Experimental Section

Materials: Octamethylcyclotetrasiloxane (D_4 , 98%, Sigma-Aldrich), toluene (99.7, Sigma-Aldrich), triflic acid (Sigma-Aldrich), and conductive resin (Farnell) were used as purchased. Carbon black pearls 2000 (BP-2000) was offered by Cabot Corporation. D_4 -based crosslinker ($triD_4$) was synthesized according to the method reported previously.

Fabrication and Reconfiguration of CB/dPDMS Composites: Taking CB(1)/dPDMS(1), for example, the mixture of 0.02 g Carbon black powders and 2 g D_4 monomer containing 1 wt% crosslinker in 5 g toluene was subjected to ultrasonication for 30 min, followed by addition of 20 μ L triflic acid under stirring. The mixture was then put in hood at room temperature to allow the solvent to evaporate without stirring, to get an elastic solid material. The sample was stored in a sealed glass bottle before use. The same process was used to prepare the samples with different CB contents under different conditions.

To reconfigure the CB/dPDMS composites, the materials were bonded on glass slide by 502 glues (Figure S4, Supporting Information), and then stretched and fixed at different strains in a closed container for 24 h.

Recycle of Dynamic CB/dPDMS Composites: For example, a piece of CB(1)/dPDMS(1) film (2 g) was put into the mixture of 15 g toluene containing. The mixture was stirred at room temperature for 12 h. The composite was dissolved in 12 h, resulting in a suspending solution. The mixture solution was then evaporated in hood to remove the solvent and a new CB-PDMS composite formed again.

SEM Observation: SEM images were performed on a FEI Quanta 400 FEG-ESEM with an operating voltage of 10.0 kV. The CB/dPDMS composites were cut by knife and the cross-sections of the samples were subjected to the SEM directly for observation (without gold sputtering).

Zeta Potential Measurement: To the mixture of 0.02 g CB in 5 g toluene was added 20 μ L triflic acid, followed by 1 min ultrasonication. The suspending mixture of 0.02 g CB in 5 g toluene was used as control sample. The samples were then centrifuged to collect the particles. Toluene was used to rinse the particles for three times. After drying, the obtained CB particles were dispersed in water for the zeta potential measurement (0.125 mg mL⁻¹). The zeta potential for the acid-treated CB is 3.77 \pm 0.70 mV, while that of control CB is -27.4 \pm 0.69 mV.

Rheological Characterizations: Rheological measurements were obtained using a TA instruments discovery hybrid rheometer with a PP8, 8 mm diameter parallel plate geometry with a rough surface. The dynamic modulus versus the oscillation strain rates were performed at the frequency of 1 Hz, while the dynamic modulus versus frequency were performed with the strain of 1%.

GC-MS and Chromatography Measurements: Gas chromatography mass spectrometry was performed by GC-MS Shimadzu QP 2010 using ZB-5HT-Inferno columns. The number-average molecular weight (M_n) and polydispersity index were measured by Agilent HPC chromatography (GPC) system using a ZB-5HT-Inferno column with a series of silicone oils as standard samples. The concentration for GS-MS and GPC was 1 mg mL⁻¹ in toluene.

Mechanical Tests: Mechanical tensile-stress experiments were performed on a Zwick 1446 (Zwick/Roell, Germany) at room temperature

at a loading speed of 20 mm min⁻¹. The initial gauge section is 20 mm. The specimens were 30 mm in length, 4 mm in width and 0.75 mm in thickness. The samples for the measurement of the E-modulus were stretched to break, and the E-modulus were calculated by the slope between the stress and the strain in the strain ranges of 5–10%.

Electrical Measurements: All electrical measurements were performed on the samples with a length of 30 mm, a width of 4 mm, and a thickness of 0.75 mm, using two-point probe measurements. The resistance was tracked by the GDM-8255A (GW INSTEK). Conductive epoxy A and conductive epoxy B were first mixed homogeneously with a mass ratio of 1:1. Then the mixed composites were pasted onto the surfaces to eliminate the surface effect. Copper wires were used to connect the electrode and GDM-8255A.

The conductivity was calculated by $\sigma = L/(R * S)$, where σ is the conductivity, L is the length, S is the area of the cross-section and R is the electrical resistance.

The measurements of the electrical change versus the strain were performed on Zwick 1446 to apply loads to the sensor. The assembled sensors were stuck onto the glass sides and then the glass slides were subjected to the Zwick clamps (Figure S5, Supporting Information). In this way, the effect of the force generated by the Zwick clamps on the electrical change during stretching could be avoided.

The resistance change at the fixed strains were also tracked by assembling the materials into the sensors (Figure S5) and sticking the sensors onto the glasses. A plastic wrap was coated on the surfaces of the materials that were exposed to the air during the holding (Figure S7, Supporting Information).

R-Strain Model: On one hand, the equilibrium number of interparticle connections per volume, N_1 , can be interpreted as a function of the applied tensile strain ϵ , by applying the well-known Krauss model^[41]

$$N_1 = \frac{N_0}{1 + \left(\frac{\epsilon}{\epsilon_c}\right)^{2m}} \quad (5)$$

Here, N_0 is the initial number of interparticle connections per volume, m is a constant related to the fractal structure of the network and ϵ_c is a constant which can be interpreted as the yield strain.

On the other hand, the viscous behavior of the polymer matrix enables the rearrangement of the filler particles, which additionally contributes to the interparticle connections. The number of interparticle connections per volume due to the rearrangement, N_2 , increases linearly with time.

$$N_2 = k_2 t = k_2 \epsilon / \epsilon_r \quad (6)$$

where ϵ_r is strain rate, k_2 is reforming constant because of the rearrangement. Then, at any given strain, the total number of interparticle connections per volume was given by $N = N_1 + N_2$. By analogy with percolation theory, the resistivity was given by

$$\rho = (N - N_c)^{-n_\epsilon} \quad (7)$$

N_c is the threshold value when the first conductive path occurs and n_ϵ was a scaling exponent. When the filler loading was high enough, $N \gg N_c$ and an approximation was made,

$$\rho = (N)^{-n_\epsilon} = (N_1 + N_2)^{-n_\epsilon} \quad (8)$$

Combining these equations gives

$$\rho = \frac{\rho_0}{\left[\left(1 + \left(\frac{\epsilon}{\epsilon_c} \right)^{2m} \right)^{-1} + \frac{\epsilon}{\epsilon_t} \right]^{n_\epsilon}} \quad (9)$$

where ρ_0 is the resistivity when there is no strain and $\epsilon_t = \epsilon_r N_0 / k_2$.

Combining the definition of resistance ($R = \rho L / S$) with the assumption that the volume remains constant under deformation ($S_0 L_0 = SL$) and

the definition of strain ($\Delta L/L_0 = \varepsilon$) allows to relate the material resistivity to the strain-dependent resistance:

$$\rho = RS_0 L_0^{-1} (\varepsilon + 1)^2 \quad (10)$$

$$\frac{R}{R_0} = \left[\left(1 + \left(\frac{\varepsilon}{\varepsilon_c} \right)^{2m} \right)^{-1} + k_2 t / N_0 \right]^{-n_e} (\varepsilon + 1)^2 \quad (11)$$

Supporting Information

Supporting Information is available from the Wiley Online Library or from the author.

Acknowledgements

The work was financially supported by the Bundesministerium für Bildung und Forschung under award number 031A360D; X.Z. acknowledges support from Chinese Scholarship Council (CSC) and H.Z. acknowledges fellowship supported by the Alexander von Humboldt Foundation. The authors also thank Rebekka Christmann from Helmholtz-Institute for Pharmaceutical Research Saarland (HIPS)-Helmholtz Centre for Infection Research (HZI) for the zeta potential measurement.

Conflict of Interest

The authors declare no conflict of interest.

Keywords

dynamic polymer composites, post-tunable sensitivity, recyclable sensors, self-healable, tactile force sensors

Received: April 22, 2020

Revised: May 24, 2020

Published online: July 15, 2020

- [1] F. Ilievski, A. D. Mazzeo, R. F. Shepherd, X. Chen, G. M. Whitesides, *Angew. Chem., Int. Ed.* **2011**, *50*, 1890.
- [2] B. T. Nghiem, I. C. Sando, R. B. Gillespie, B. L. McLaughlin, G. J. Gerling, N. B. Langhals, M. G. Urbanek, P. S. Cederna, *Plast. Reconstr. Surg.* **2015**, *135*, 1652.
- [3] C. Antfolk, M. D'alonzo, B. Rosén, G. Lundborg, F. Sebelius, C. Cipriani, *Expert Rev. Med. Devices* **2013**, *10*, 45.
- [4] D. Son, J. Lee, S. Qiao, R. Ghaffari, J. Kim, J. E. Lee, C. Song, S. J. Kim, D. J. Lee, S. W. Jun, S. Yang, M. Park, J. Shin, K. Do, M. Lee, K. Kang, C. S. Hwang, N. Lu, T. Hyeon, D.-H. Kim, *Nat. Nanotechnol.* **2014**, *9*, 397.
- [5] R. C. Webb, A. P. Bonifas, A. Behnaz, Y. Zhang, K. J. Yu, H. Cheng, M. Shi, Z. Bian, Z. Liu, Y.-S. Kim, W.-H. Yeo, J. S. Park, J. Song, Y. Li, Y. Huang, A. M. Gorbach, J. A. Rogers, *Sci. Adv.* **2015**, *1*, e1500701.
- [6] S. Choi, J. Park, W. Hyun, J. Kim, J. Kim, Y. B. Lee, C. Song, H. J. Hwang, J. H. Kim, T. Hyeon, D.-H. Kim, *ACS Nano* **2015**, *9*, 662.
- [7] R. S. Dahiya, G. Metta, M. Valle, G. Sandini, *IEEE Transact. Robot.* **2009**, *26*, 1.
- [8] R. S. Johansson, J. R. Flanagan, *Nat. Rev. Neurosci.* **2009**, *10*, 345.
- [9] V. E. Abaira, D. D. Ginty, *Neuron* **2013**, *79*, 618.
- [10] L. Lin, S. Liu, Q. Zhang, X. Li, M. Ji, H. Deng, Q. Fu, *ACS Appl. Mater. Interfaces* **2013**, *5*, 5815.
- [11] J.-Y. Jeon, T.-J. Ha, *ACS Appl. Mater. Interfaces* **2016**, *8*, 2866.
- [12] Y. Hu, T. Zhao, P. Zhu, Y. Zhang, X. Liang, R. Sun, C.-P. Wong, *Nano Res.* **2018**, *11*, 1938.
- [13] L.-Q. Tao, D.-Y. Wang, H. Tian, Z.-Y. Ju, Y. Liu, Y. Pang, Y.-Q. Chen, Y. Yang, T.-L. Ren, *Nanoscale* **2017**, *9*, 8266.
- [14] J. Hwang, J. Jang, K. Hong, K. N. Kim, J. H. Han, K. Shin, C. E. Park, *Carbon* **2011**, *49*, 106.
- [15] Z. Wang, X. Liu, X. Shen, N. M. Han, Y. Wu, Q. Zheng, J. Jia, N. Wang, J. K. Kim, *Adv. Funct. Mater.* **2018**, *28*, 1707043.
- [16] S. C. Mannsfeld, B. C. Tee, R. M. Stoltenberg, C. V. H. Chen, S. Barman, B. V. Muir, A. N. Sokolov, C. Reese, Z. Bao, *Nat. Mater.* **2010**, *9*, 859.
- [17] B. C. K. Tee, A. Chortos, R. R. Dunn, G. Schwartz, E. Eason, Z. Bao, *Adv. Funct. Mater.* **2014**, *24*, 5427.
- [18] Z. Wang, Q. Zhang, Y. Yue, J. Xu, W. Xu, X. Sun, Y. Chen, J. Jiang, Y. Liu, *Nanotechnology* **2019**, *30*, 345501.
- [19] X. Zeng, Z. Wang, H. Zhang, W. Yang, L. Xiang, Z. Zhao, L.-M. Peng, Y. Hu, *ACS Appl. Mater. Interfaces* **2019**, *11*, 21218.
- [20] B. C. Tee, C. Wang, R. Allen, Z. Bao, *Nat. Nanotechnol.* **2012**, *7*, 825.
- [21] Z. Zou, C. Zhu, Y. Li, X. Lei, W. Zhang, J. Xiao, *Sci. Adv.* **2018**, *4*, eaq0508.
- [22] Z. Q. Lei, P. Xie, M. Z. Rong, M. Q. Zhang, *J. Mater. Chem. A* **2015**, *3*, 19662.
- [23] N. N. Xia, X. M. Xiong, J. Wang, M. Z. Rong, M. Q. Zhang, *Chem. Sci.* **2016**, *7*, 2736.
- [24] C. S. Boland, U. Khan, G. Ryan, S. Barwich, R. Charifou, A. Harvey, C. Backes, Z. Li, M. S. Ferreira, M. E. Möbius, R. J. Young, J. N. Coleman, *Science* **2016**, *354*, 1257.
- [25] S. H. Kim, H. Seo, J. Kang, J. Hong, D. Seong, H.-J. Kim, J. Kim, J. Mun, I. Youn, J. Kim, Y.-C. Kim, H.-K. Seok, C. Lee, J. B.-H. Tok, Z. N. Bao, D. Son, *ACS Nano* **2019**, *13*, 6531.
- [26] Q. Wu, H. Xiong, Y. Peng, Y. Yang, J. Kang, G. Huang, X. Ren, J. Wu, *ACS Appl. Mater. Interfaces* **2019**, *11*, 19534.
- [27] J. Zhou, P. Han, M. Liu, H. Zhou, Y. Zhang, J. Jiang, P. Liu, Y. Wei, Y. Song, X. Yao, *Angew. Chem., Int. Ed.* **2017**, *56*, 10462.
- [28] P. Han, X. He, Y. Zhang, H. Zhou, M. Liu, N. Wu, J. Jiang, Y. Wei, X. Yao, J. Zhou, *Adv. Opt. Mater.* **2019**, *7*, 1801749.
- [29] D. Zhang, S. Xu, X. Zhao, W. Qian, C. R. Bowen, Y. Yang, *Adv. Funct. Mater.* **2020**, *30*, 1910809.
- [30] J. Jiang, B. Bao, M. Li, J. Sun, C. Zhang, Y. Li, F. Li, X. Yao, Y. Song, *Adv. Mater.* **2016**, *28*, 1420.
- [31] S. W. Kantor, W. T. Grubb, R. C. Osthoff, *J. Am. Chem. Soc.* **1954**, *76*, 5190.
- [32] R. Xu, C. Wu, H. Xu, *Carbon* **2007**, *45*, 2806.
- [33] J. Li, P. C. Ma, W. S. Chow, C. K. To, B. Z. Tang, J. K. Kim, *Adv. Funct. Mater.* **2007**, *17*, 3207.
- [34] P. M. Kogut, J. P. Straley, *J. Phys. Condens. Matter* **1979**, *12*, 2151.
- [35] S. Shang, Y. Yue, X. Wang, *Rev. Sci. Instrum.* **2016**, *87*, 123910.
- [36] P. Cassagnau, *Polymer* **2003**, *44*, 2455.
- [37] T. Yang, D. Xie, Z. Li, H. Zhu, *Mater. Sci. Eng.: R: Reports* **2017**, *115*, 1.
- [38] L. Wang, Y. Han, C. Wu, Y. Huang, *Smart Mater. Struct.* **2013**, *22*, 075021.
- [39] B. H. Cipriano, A. K. Kota, A. L. Gershon, C. J. Laskowski, T. Kashiwagi, H. A. Bruck, S. R. Raghavan, *Polymer* **2008**, *49*, 4846.
- [40] E. Bilotti, H. Zhang, H. Deng, R. Zhang, Q. Fu, T. Peijs, *Compos. Sci. Technol.* **2013**, *74*, 85.
- [41] G. Kraus, *J. Appl. Polym. Sci. Symp.* **1984**, *39*, 75.